UDC 631.311:629.3.027.4:539.3
DOI: 10.15587/2706-5448.2025.346717

Volodymyr Kovbasa,
Nataliia Priliepo

ANALYTICAL DETERMINATION OF ABSOLUTE DEFORMATIONS AND BOUNDARIES OF THE CONTACT ZONE OF A DEFORMABLE WHEEL WITH A DEFORMABLE SURFACE

The object of research is the contact interaction between a deformable wheel (tire) and a deformable supporting surface. One of the most problematic areas is defining the boundaries of the contact zone as a function of applied loads, wheel geometry, and the mechanical properties of the contacting surfaces, as well as the increasing need to reduce energy consumption and soil compaction in the context of vehicle running gear systems.

During the research, methods from the mechanics of continuous deformable media were used to identify the deformable properties of contacting surfaces. The investigations were founded on previously published research concerning the distribution of contact forces, obtained using biharmonic potential analytical functions based on methods employed by Boussinesq and Cerruti.

Analytical dependencies have been derived that relate the leading and trailing edges of the deformable wheel's (tire's) contact with the deformable surface. This is because the proposed approach, which considers the relationship between forces and displacements on the surface and deformations and stresses within the contacting bodies, taking into account their mechanical properties, is more informative compared to methods of theoretical and analytical mechanics. The research revealed that the potential for improving the object's functioning lies in optimizing the selection of parameters and operating modes for running gear systems.

Thanks to this, it becomes possible to obtain optimized values for the geometric size of the contact surface. Compared to analogous known approaches, this ensures an enhancement in the tractive efficiency of driving wheels, minimizing wheel slip to acceptable levels, which directly addresses key challenges in agricultural and off-road machinery by contributing to reduced energy consumption and soil compaction.

Keywords: *deformable wheel, deformable support surface, absolute deformations, contact zone boundaries.*

Received: 29.09.2025
Received in revised form: 23.11.2025
Accepted: 14.12.2025
Published: 29.12.2025

How to cite
Kovbasa, V., Priliepo, N. (2025). Analytical determination of absolute deformations and boundaries of the contact zone of a deformable wheel with a deformable surface. Technology Audit and Production Reserves, 6 (1 (86)), 26–33. https://doi.org/10.15587/2706-5448.2025.346717

1. Introduction

The accuracy in defining the boundaries of the contact zone between deformable bodies with individual geometries in contact mechanics is a decisive part of many thematic publications. Quite logically, within this contact zone, the interacting bodies are under deformation, so the challenge lies in the correct analysis of the existing boundaries, especially when the interacting bodies have different Poisson's ratios and moduli of elasticity.

The basic principles, mathematical tools, and theories can be found in the fundamental work of contact mechanics [1] that influenced the development of existing methods for determining the contact zones [2]. Empirical methods use experiments that are done under specific conditions of load, material properties, and geometry. Well-known numerical methods, such as FEM (Finite Element Method) or DEM (Discrete Element Method) are able to determine specific contact characteristics for the conditions mentioned above. Both methods are widely used.

For example, this study [3] showed an interesting experiment for observing a tire deformation in real time. A system of high-speed cameras and a specially made stability aid was used to create a 3D profile of the tire and its deformations, showing promising data for characteristics of the contact zone. Such experiments are important for getting results in real-life conditions, cause later they can be used for more in-depth numerical models. In contrast, they are often focused on developing simulations used for explaining the tire-soil interactions [4]. These simulations can be proven accurate through comparison with existing test results for soil particle mobility that show significant likeness between empirical and numerical data. At the same time, formulating general dependencies for contact zone interactions needs using both extensive experiments and difficult mathematical calculations that are inconvenient and excessive [5]. Furthermore, the reliability of the obtained results can vary due to the starting hypothesis.

Analytical methods for solving elastic contact problems often use the functions of Boussinesq and Cerruti. They provide basic mathematical solutions for concentrated normal and tangential loads, showing an important beginning for later analysis [6]. All these studies are used for further advancement in the circuit. Specific geometries, material properties, and applied loads are the basis for modelling equations for contact zones and rolling resistance of the wheel-support surface interactions [7]. A considerably new study shows how using biharmonic functions that take into account equations for distributed and concentrated forces can determine the force distribution at the contact zone [8].

But using only simplified assumptions and selective omissions can significantly influence the predictive accuracy. This study [9] demonstrates

valid experimentation that shows how ESWL (Equivalent Single-Wheel Load) simplifies pavement design, combining multiple loads into one, neglecting critical present longitudinal and transversal stresses. In the same manner, existing empirical models can be found efficient, but lacking in taking into consideration complex non-linear relationships in deformations in the wheel-soil contact zone, potentially leading to faulty mobility predictions [10].

One of the most important parameters of possible solutions is the boundaries of the contact zone, because of its significance in describing force distributions, body deformation, and internal stresses. These boundaries are, in turn, functions of the applied loads, the mechanical properties, and geometry of the interacting bodies. Therefore, developing a sound method for determining these boundaries is pivotal for the circuit of contact mechanics.

Thus, *the object of research* is the contact interaction between a deformable wheel (tire) and a deformable supporting surface.

The aim of research is to establish an analytical relationship for determining the boundaries of the contact zone as a function of applied loads, the geometric parameters of the wheel, and the mechanical properties of the contacting surfaces.

The tasks of this research were as follows:

1) to determine the absolute vertical components of deformation for both the tire and the supporting surface, based on the dependencies presented in the previous publication;

2) to ascertain the magnitude of the maximum absolute vertical deformation of the deformed tire at the trailing edge of the contact patch, considering that the deformation of the supporting surface at this point is finite;

3) to determine the horizontal boundary of the finite tire deformation at the trailing edge of the contact patch;

4) to determine the leading edge of the contact zone, given the known magnitude of the trailing edge and considering that the cumulative deformation of the tire and the supporting surface at this point is zero and derive the final equations for the boundaries of the leading and trailing contact points.

2. Materials and Methods

This research extends the work initiated in paper [8] on the contact interaction between a deformable wheel (tire) and a deformable surface. The primary objective of this extension is to establish analytical expressions for the absolute deformations of both the wheel and the supporting surface. These expressions are critical, as they can be analytically transformed to define the boundaries of the contact zone as a function of applied loads, wheel geometry, and the mechanical properties of the interacting materials.

The methodology leverages analytical force distributions previously developed for non-conforming bodies. These are integrated with transformed Boussinesq and Cerruti equations [8] within a planar problem formulation. This synthesis yields the components of absolute deformation for both the wheel and the supporting surface. Crucially, these deformation components are biharmonic analytical functions, representing the solution to the first boundary value problem for a half-space. As the initial force distributions are functions of the system's loads, geometry, and material properties, the resulting deformation fields are likewise dependent on these same parameters.

This analytical approach offers significant advantages over purely numerical or experimental methods. It provides a more general solution, offers deeper insight into the underlying physical mechanisms of contact, and furnishes a robust foundation for subsequent theoretical developments and parametric studies.

The general case of the interaction between a deformable wheel and soil, which considers all the acting forces, is shown in Fig. 1. This model can be used for both driving and passive wheels.

The mathematical equations for absolute surface deformation previously published in paper [7], made for a planar problem, can be used as the basis for created analytical relationships for displacement. At the same time, these relationships allow for a systematic analysis of the resulting deformation. They also can look into key parameters and surface properties that influence these deformations.

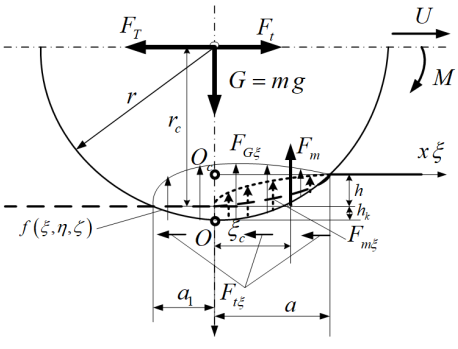

Fig. 1. Schematic of the wheel-soil interaction, illustrating the forces in the general case for both driving and passive wheel conditions

Fig. 1 illustrates the interaction scheme of a deformable wheel within the $\xi\zeta$ coordinate system, which coincides with the xz coordinate system of the deformable surface. The division of the coordinate systems is made to allow for the description of the geometric parameters of both the wheel and support surfaces.

The following forces act on the wheel's center of rotation: the weight acting on the wheel $G = mg$, the pushing force (for a passive wheel) exerted from the frame F_b, the traction force applied to the wheel from the frame caused by the tractive force F_T, and the torque that causes the wheel to rotate (for the active wheel, for the passive wheel $M = 0$).

The distributed forces in the wheel-surface contact zone are designated as follows: F_m – wheel rolling resistance, where the action center is located at a ξ_c distance from the wheel axis. The symbol U indicates the direction of the wheel's movement.

The geometric parameters of the contact zone interaction are as follows: a, a_1 – the front and the rear contact boundaries, h – the support surface deformation, h_k – deformation of the deformable wheel [8]. The presented solution is a continuation of the previously published study [8].

3. Results and Discussion

Vertical displacements of the wheel surface:

$$w_{k\xi\eta} = -\frac{1}{4G_k\pi}\times$$
$$\times\int_{b_1}^{b}\int_{a_1}^{a}\left(1-\frac{2\xi^2}{r^2}-\frac{2k^4\eta^2\left(r^2-6\xi^2\right)}{r^4}\right)\left(\frac{F_{zkk}\left(-3+2\nu_k\right)}{\sqrt{z^2+\left(y-\eta\right)^2+\left(x-\xi\right)^2}}+\frac{\left(-1+2\nu_k\right)F_{xkk}}{\sqrt{z^2+\left(y-\eta\right)^2+\left(x-\xi\right)^2}}\right)\mathrm{d}\xi\,\mathrm{d}\eta;$$
$$F_{xkk} = \frac{F_t - F_T + ftgm + \dfrac{M_c}{h_k - r}}{\left(a-a_1\right)\left(b-b_1\right)},$$
$$F_{zkk} = \frac{-a_1M_c + a^2\left(F_{Tk} + \dfrac{a_1F_t}{h_k-r}\right) + a\left(\begin{matrix}-a_1\left(F_{Tk}+gm\right)+\\ +M_c+\dfrac{a_1^2F_t}{-h_k+r}\end{matrix}\right)}{a\left(a-a_1\right)a_1\left(b-b_1\right)}, \qquad (1)$$

where G_k – elastic modulus of the wheel material; a, a_1 – front and rear contact boundaries; ν_k – Poisson's ratio of the wheel material; b, b_1 – transverse wheel boundaries (axis $OyidemO\eta$); r – wheel radius;

ISSN-L 2664-9969; E-ISSN 2706-5448

ξ – longitudinal coordinate of the deformable wheel system; k – coefficient characterizing the ellipticity of the contact zone surface; η – transverse coordinate of the deformable wheel system; x – longitudinal axis of the coordinate system under consideration; y – transverse axis of the coordinate system under consideration; z – vertical axis of the coordinate system under consideration; d – final total deformation of the supporting surface; F_{zkk} – component of the total function for the vertically distributed forces acting on the wheels; F_{xkk} – component of the total function for the horizontally distributed forces acting on the wheels; F_T – tractive force; F_t – pushing force; g – gravitational acceleration; m – mass per wheel; M_c – torque; h_k – component of the final deformation of the deformable wheel.

The fully expanded analytical solution to this integral is omitted due to its considerable length and complexity. However, the solution can be evaluated numerically to visualize the deformation profile. Fig. 2 illustrates the resulting vertical displacement of the wheel surface across the contact zone.

An analysis of the vertical wheel deformation, governed by (1) and illustrated in Fig. 2, reveals the influence of key system parameters on the magnitude of displacement. The primary relationships observed are that the magnitude of the wheel's absolute surface deformation increases with increases in the applied torque M_c, tractive force F_T, and mass m. Conversely, an increase in the wheel's surface elastic modulus G_k results in a decrease in the vertical deformation component.

Vertical displacements of the support surface in the contact zone:

$$w_{n\xi\eta} = \int_{b_1}^{b}\left(\int_{a_1}^{1}\left(-\frac{2\eta^2k^4\left(r^2-6\xi^2\right)}{r^4}-\frac{2\xi^2}{r^2}+1\right)\left(\frac{F_{xnn}\left(2\nu_n-1\right)}{\sqrt{\left(x-\xi\right)^2+\left(y-\eta\right)^2+z^2}}+\frac{F_{znn}\left(2\nu_n-3\right)}{\sqrt{\left(x-\xi\right)^2+\left(y-\eta\right)^2+z^2}}\right)\mathrm{d}\xi\right)\mathrm{d}\eta = -\frac{}{4\pi G_n};$$

$$F_{xnn}=\frac{F_t-F_T+\dfrac{M_c+f_tgm\left(h-r\right)}{h-r}}{\left(a-a_1\right)\left(b-b_1\right)},$$

$$F_{znn}=\frac{a^2a_1\left(F_t+F_T\right)+2a_1M_c\left(-h+r\right)-a\begin{pmatrix}a_1^2\left(F_t+F_T\right)+\\-a_1gm\left(h-r\right)+\\+2M_c\left(-h+r\right)\end{pmatrix}}{a\left(a-a_1\right)a_1\left(b-b_1\right)\left(-h+r\right)}, \quad (2)$$

where G_n – elastic modulus of shear deformation of the support surface; ν_n – Poisson's ratio of the support surface; F_{xnn} – component of the total function for the horizontally distributed forces acting on the supporting surface; F_{znn} – component of the total function for the vertically distributed forces acting on the supporting surface, h – component of the final deformation of the deformable supporting surface.

Fig. 3 illustrates the resulting vertical displacement of the support surface across the contact zone.

Analysis of the vertical deformation of the support surface, as described by (2) and visualized in Fig. 3, yields the following key findings: the absolute deformation of the support surface increases with an increase in any of the applied loads. This includes the wheel torque M_c, tractive force F_T, pushing force F_t (for a passive wheel), and mass m per wheel. An increase in the elastic modulus of the support surface G_n results in reduced vertical deformation. As expected, a stiffer surface material is more resistant to indentation under load.

Increasing the wheel radius r leads to a decrease in deformation of the support surface. This occurs because a larger radius distributes the vertical load over a longer contact patch, which reduces the peak contact pressure exerted on the surface.

Horizontal movements of the wheel surface:

$$u_{k\xi\eta} = -\frac{1}{4G_k\pi}\times$$

$$\times\int_{b_1}^{b}\int_{a_1}^{a}\left(1-\frac{2\xi^2}{r^2}-\frac{2k^4\eta^2\left(r^2-6\xi^2\right)}{r^4}\right)\left(\frac{F_{zkk}\left(2\nu_k-1\right)}{\sqrt{z^2+\left(y-\eta\right)^2+\left(x-\xi\right)^2}}+\frac{F_{xkk}\left(2\nu_k-3\right)}{\sqrt{z^2+\left(y-\eta\right)^2+\left(x-\xi\right)^2}}\right)\mathrm{d}\xi\mathrm{d}\eta;$$

$$F_{xkk}=\frac{F_t-F_T+f_tgm+\dfrac{M_c}{h_k-r}}{\left(a-a_1\right)\left(b-b_1\right)},$$

$$F_{zkk}=\frac{-a_1M_c+a^2\left(F_T+\dfrac{a_1F_t}{h_k-r}\right)+a\begin{pmatrix}-a_1\left(F_T+gm\right)+\\+M_c+\dfrac{a_1^2F_t}{-h_k+r}\end{pmatrix}}{a\left(a-a_1\right)a_1\left(b-b_1\right)}. \quad (3)$$

Fig. 4 illustrates the horizontal displacement profile of the wheel surface within the contact zone.

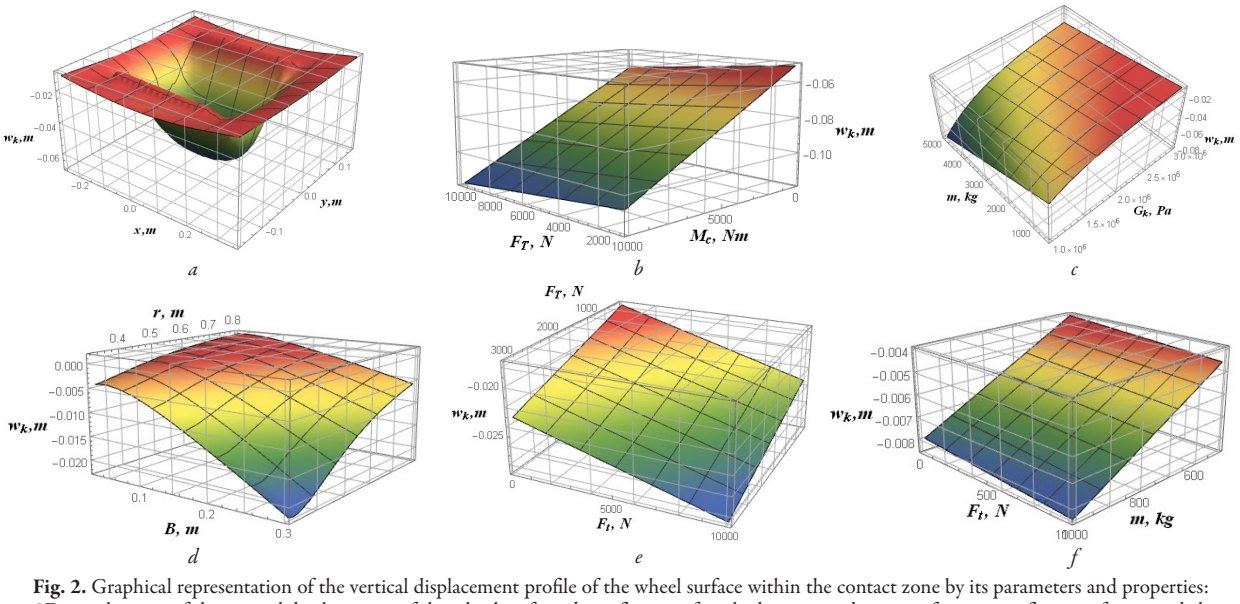

a b c d e f

Fig. 2. Graphical representation of the vertical displacement profile of the wheel surface within the contact zone by its parameters and properties: *a* – 3D visualization of the vertical displacement of the wheel surface; *b* – influence of applied torque and traction force; *c* – influence of mass and elastic modulus of the wheel; *d* – influence of width and radius of the wheel; *e* – influence of traction and pushing forces; *f* – influence of mass and pushing force

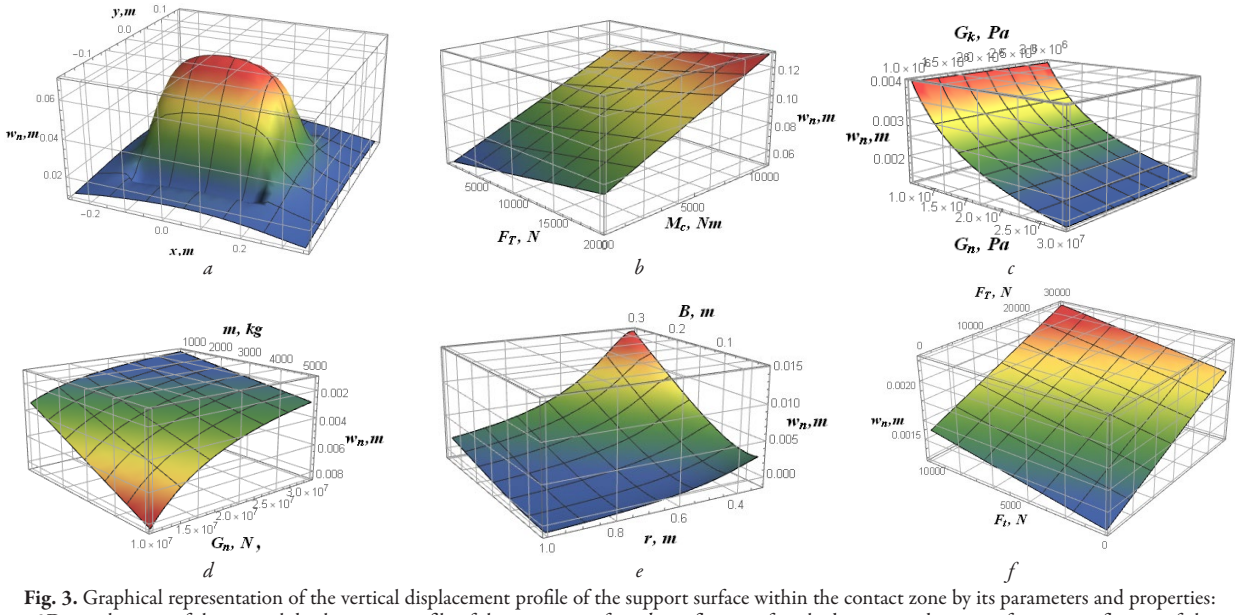

Fig. 3. Graphical representation of the vertical displacement profile of the support surface within the contact zone by its parameters and properties: *a* – 3D visualization of the vertical displacement profile of the support surface; *b* – influence of applied torque and traction force; *c* – influence of elastic moduli of the wheel material and support surface; *d* – influence of mass and elastic modulus of the support surface; *e* – influence of width and radius of the wheel; *f* – influence of traction and pushing forces

Arriving from (3), Fig. 4 demonstrates the following dependencies: horizontal deformations increase with the increase in the applied torque M_c, tractive force F_T, pushing force F_t (for a passive wheel), and mass m per wheel. This increase will cause the wheel to deform horizontally, as it'll initiate the shear stresses in the contact zone.

Contrarily, an increase in the wheel's elastic modulus G_k or its radius r will lead to a decrease in horizontal deformations, as a larger radius can change the distribution of shear stresses.

Horizontal displacements of the support surface in the contact zone:

$$u_{n\xi\eta} = \int_{b_1}^{1}\left(\int_{a_1}^{a}\left(-\frac{2\eta^2k^4\left(r^2-6\xi^2\right)}{r^4}-\frac{2\xi^2}{r^2}+1\right)\left(\frac{F_{xnn}\left(2\nu_n-3\right)}{\sqrt{\left(x-\xi\right)^2+\left(y-\eta\right)^2+z^2}}+\frac{F_{znn}\left(2\nu_n-1\right)}{\sqrt{\left(x-\xi\right)^2+\left(y-\eta\right)^2+z^2}}\right)d\xi\right)d\eta = -\frac{}{4\pi G_n};$$

$$F_{xnn}=\frac{F_t-F_T+\dfrac{M_c+f_tgm\left(h-r\right)}{h-r}}{\left(a-a_1\right)\left(b-b_1\right)},$$

$$F_{znn}=\frac{a^2a_1\left(F_t+F_T\right)+2a_1M_c\left(-h+r\right)-a\begin{pmatrix}a_1^2\left(F_t+F_T\right)+\\+a_1gm\left(h-r\right)+\\+2M_c\left(-h+r\right)\end{pmatrix}}{a\left(a-a_1\right)a_1\left(b-b_1\right)\left(-h+r\right)}. \quad (4)$$

Fig. 5 illustrates the horizontal displacement profile of the support surface within the contact zone.

Analyzing Fig. 5, arriving from (4), it's possible to grasp that an increase in the wheel torque M_c, the resultant tractive force F_T, the pushing force in the case of a passive wheel F_t, or the mass m per wheel leads to a more noticeable horizontal deformation of the support surface. This can be seen as a direct result of the increase in shear stress acting in the contact zone, which is needed to create traction and overcome the rolling resistance. The illustrations also show that some parameters can have an abating effect. For example, an increase in the elastic modulus of the support surface G_n boosts the material's natural resistance to shear, reducing the horizontal displacement. Similarly, increasing the wheel radius r will distribute the contact pressures and shear stresses over a larger area, which will lead to a decrease in the top deformation of the support surface.

The longitudinal range on the contact zone of the deformable wheel with the deforming surface is along the axis *OyidemOη*. This allows to look at the existing problem as a planar problem formulation. It will also simplify the equations, because under the conditions of the problem, on the rear (trailing) edge of the contact zone a_1, that is, when $x = \xi = a_1$, the maximum displacement of the wheel surface in the first approximation is $w_{k|\xi=x=a1} = a_1^2/2r$.

At the leading edge of the contact zone $x = \xi = a$, the sum of the surface displacements represents the total gap closure and is equal to zero: $w_k + w_{n|\xi=x=a} = 0$.

Determining the contact zone boundaries requires evaluating the vertical displacement fields for both the wheel and the bearing surface at the specified points.

To calculate the boundaries of the contact zone between the wheel and the support surface, it is necessary to determine the components of the vertical displacements of the wheel surface and the support surface at the contact zone boundary points $x = \xi = a_1$ and $x = \xi = a$. The vertical component of the wheel displacement is simplified under the assumption of small deformations. This allows the higher-order terms in the expression to be neglected, resulting in the form presented in (1), and given that $E = 2(1 + \nu)G$, the last expression will take the form:

$$w_k=\frac{\left(1+\nu k\right)\xi\begin{pmatrix}3F_{xkk}\pi\left(-1+2\nu_k\right)\xi\left(-r^2+\xi^2\right)+\\+F_{zkk}\left(-1+\nu_k\right)\begin{pmatrix}12x^3+6x^2\xi+4x\xi^2+\\+3\xi^3-6r^2\left(2x+\xi\right)\end{pmatrix}\end{pmatrix}}{12E_k\pi r^2};$$

$$w_ka_1=\left(w_k/.\xi=a_1\right)-\left(w_k/.\xi=a_1\right)\Big|_{x=\xi}=$$

$$=-\frac{a_1\left(1+\nu_k\right)\begin{pmatrix}F_{zkk}\left(3a_1^3-6a_1r^2\right)\left(-1+\nu_k\right)+\\+3a_1F_{xkk}\pi\left(a_1^2-r^2\right)\left(-1+2\nu_k\right)\end{pmatrix}}{12E_k\pi r^2}. \quad (5)$$

ISSN-L 2664-9969; E-ISSN 2706-5448

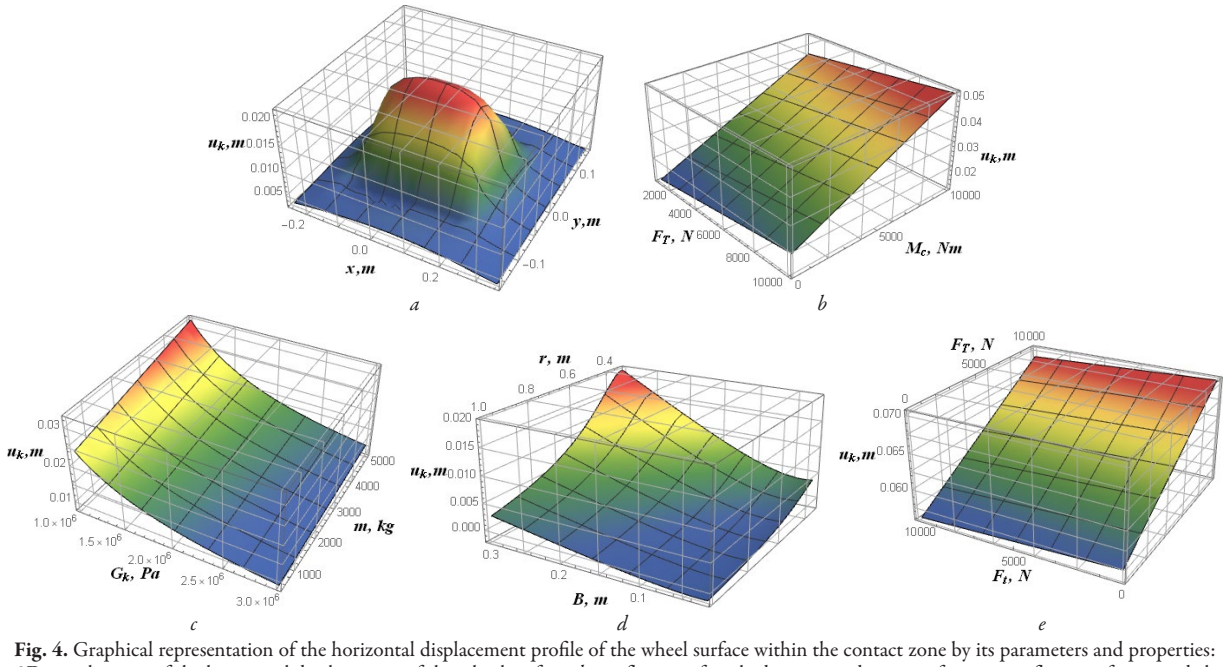

Fig. 4. Graphical representation of the horizontal displacement profile of the wheel surface within the contact zone by its parameters and properties: *a* – 3D visualization of the horizontal displacement of the wheel surface; *b* – influence of applied torque and traction force; *c* – influence of mass and elastic modulus of the wheel; *d* – influence of width and radius of the wheel; *e* – influence of traction and pushing forces

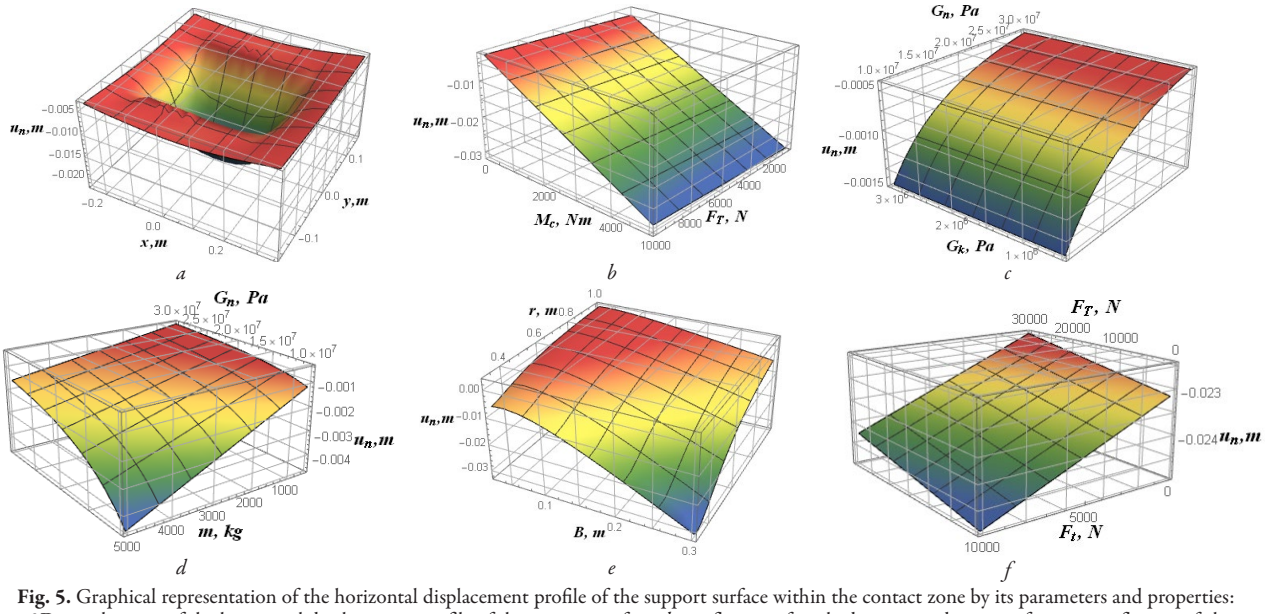

Fig. 5. Graphical representation of the horizontal displacement profile of the support surface within the contact zone by its parameters and properties: *a* – 3D visualization of the horizontal displacement profile of the support surface; *b* – influence of applied torque and traction force; *c* – influence of elastic moduli of the wheel material and support surface; *d* – influence of mass and elastic modulus of the support surface; *e* – influence of width and radius of the wheel; *f* – influence of traction and pushing forces

Equating the previously derived expression with the vertical wheel deformation at the point a_1: $w_{k|\xi=x=a1}=a_1^2/2r$, and subsequently solving the resulting equation for a_1, it is possible to obtain an expression for the coordinate of the rear boundary of the contact zone

$$a_1=\begin{pmatrix}2(\nu k^2-1)r(h_k-r)\times\\ \times(aF_T+M_c)\end{pmatrix}\Big/\begin{pmatrix}2a(\pi BE_k(h_k-r)-F_t(\nu_k{}^2-1)r)-\\ -(\nu_k+1)r\begin{pmatrix}gm(\pi f_t(2\nu_k-1)-\\ -2\nu_k+2\end{pmatrix}\times\\ \times(h_k-r)+\pi(2\nu_k-1)\times\\ \times\begin{pmatrix}F_t(h_k-r)+\\ +F_T(r-h_k)+M_c\end{pmatrix}\end{pmatrix}. \quad (6)$$

The dependency of the rear contact boundary's location on key wheel parameters is illustrated in Fig. 6.

The analysis of the dependence illustrates that:
– with an increase in the wheel radius r, the length of the rear boundary of the contact zone a_1 increases linearly;
– with an increase in the wheel's modulus of curvature E_k, the contact area a_1 decreases inversely;
– with increasing tractor mass applied to the wheel m, the size of the rear boundary of the contact area a_1 decreases linearly;
– with increasing tractive force F_T, the coordinate of the rear boundary of the contact area a_1 increases linearly;
– with a decrease in the width of the wheel B, the coordinate of the rear boundary of the contact zone a_1 increases inversely;
– an increase in the applied torque M_c leads to a non-linear increase in the rear boundary coordinate a_1.

To determine the front boundary of the contact zone, the functions of the sum of the vertical displacements of the wheel and the

bearing surface from (1) and (2) must be reduced to zero at $x = \xi = a$. An expression for the coordinate of the front boundary is derived by applying the governing contact condition $w_k + w_{n|\xi=x=a} = 0$ and using the solution for the rear boundary a_1. This final expression is simplified by neglecting higher-order terms, which are considered insignificant for this analysis, but taking into account that $E = 2(1 + \nu)G$

$$a = -\left(\begin{pmatrix} 2M_c(h-r)(r-h_k)\times \\ \times\begin{pmatrix} 2E_k(\nu n^2-1)+ \\ +E_n(\nu k^2-1)\end{pmatrix}\end{pmatrix} \Big/ \left(-2a_1\begin{pmatrix} E_k(\nu n^2-1)\times \\ \times(F_t+F_T)(h_k-r)+ \\ +E_nF_t(\nu k^2-1)(h-r)\end{pmatrix}+\right.$$
$$+E_k(\nu n+1)(h_k-r)\begin{pmatrix} -gm(\pi f_t(2\nu n-1)+2(\nu n-1))(h-r)- \\ -\pi(2\nu n-1)(F_t(h-r)-F_Th+F_Tr+M_c)\end{pmatrix}+$$
$$\left.+E_n(\nu k+1)(h-r)\begin{pmatrix} gm(\pi f_t(2\nu k-1)-2\nu k+2)(h_k-r)+ \\ +\pi(2\nu k-1)(F_t(h_k-r)+M_c)- \\ -F_T(2\pi\nu k+2\nu k-\pi-2)(h_k-r)\end{pmatrix}\right). \quad (7)$$

Fig. 7 illustrates how the location of the front boundary varies as a function of the wheel's geometric and material properties.

The analysis of the dependence illustrates that:

– the modulus of wheel's curvature, E_n, is inversely proportional to the front boundary coordinate of the contact zone a;

– the front boundary of the contact zone, a, increases linearly with the applied torque M_c;

– the front boundary of the contact zone, a, increases linearly with the wheel's modulus of curvature E_k;

– the front boundary of the contact zone, a, is inversely proportional to the wheel radius r;

– the front contact boundary, a, is inversely proportional to the mass of the tractor, m, applied to the wheel;

– the position of the front contact boundary, a, shows a slight positive dependence on the applied pushing force F_t;

– the front contact boundary, a, decreases linearly as the tractive force F_T, increases.

As a result of the conducted research, analytical relationships have been derived to determine the boundaries of the contact zone as a function of applied loads, geometric parameters of the wheel, and the mechanical properties of the contacting surfaces. Based on the solutions obtained for this research objectives, the following conclusions can be drawn. The obtained analytical relationships significantly simplify the prediction of the nature of the contact interaction between two deformable bodies of non-conformal geometry. This offers a significant advantage compared to known methods of experimental research and numerical modelling using FEM and FVM methods. The latter requires substantial material costs (for experimental methods) and considerable computations (for numerical methods). The results obtained enable the investigation of slippage and sliding conditions of wheeled propulsion systems and the determination of their trafficability, given the known mechanical properties of the support surface.

The research findings presented in this publication can be practically applied to determine the dimensions of the contact patch between a deformable wheel (tire) and a deformable supporting surface, given known wheel loads, geometric dimensions, and the mechanical properties of both the tire and the supporting surface. This enables the determination of permissible loads on the supporting surface, the wheel's tractive characteristics, and allowable deformations to ensure the requisite off-road capability and tractive effort that the unit can generate.

Furthermore, in comparison to numerical solution methods, they – while possessing lower costs associated with the absence of extensive preparatory work and calculations – have sufficient accuracy. They also offer the possibility of analyzing the influence of various factors on the result and obtaining the expected nature of contact interaction at the design stage or for ensuring rational machine operating modes.

The results of the presented research open the possibility for theoretical investigations of slippage and sliding issues in the wheel-support surface contact zone, as well as for determining machine trafficability and the rational use of mobile machinery.

The research results possess certain limitations, primarily related to the necessity of determining the mechanical properties of the tire and the supporting surface. Furthermore, applying these results requires a specialist to possess knowledge of continuum mechanics for characterizing the mechanical properties of the contacting bodies, along with a university-level understanding of mathematics relevant to technical fields.

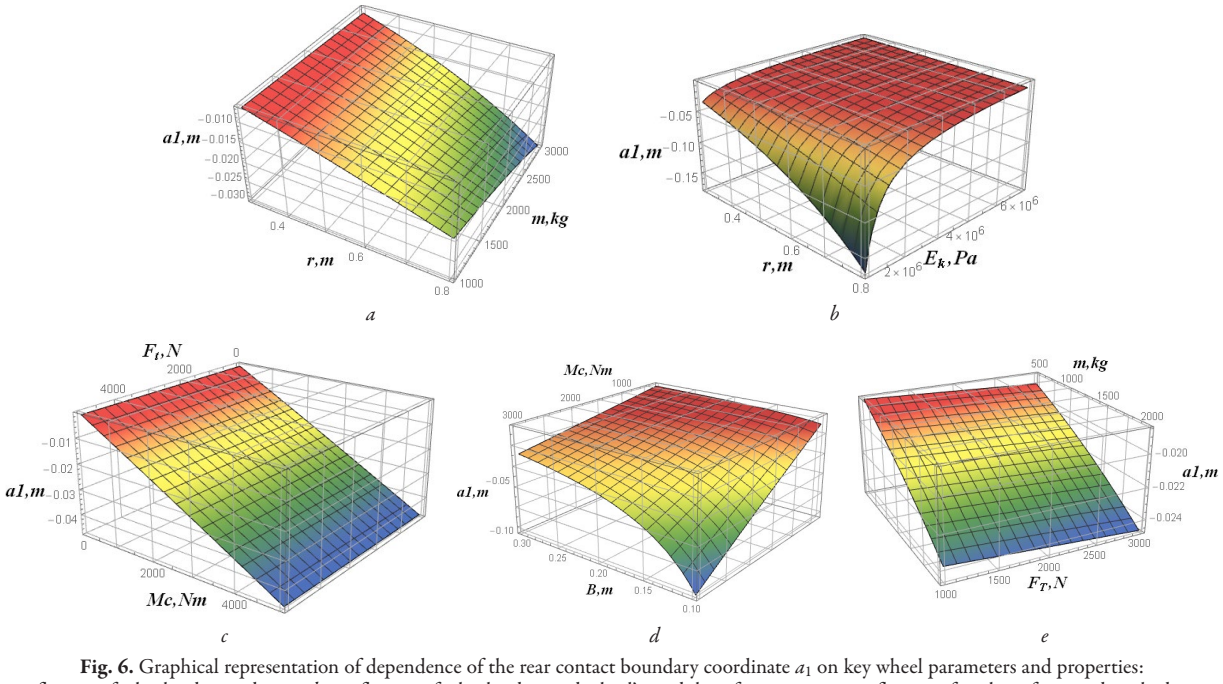

Fig. 6. Graphical representation of dependence of the rear contact boundary coordinate a_1 on key wheel parameters and properties: *a* – influence of wheel radius and mass; *b* – influence of wheel radius and wheel's modulus of curvature; *c* – influence of pushing force and applied torque; *d* – influence of applied torque and the width of the wheel; *e* – influence of traction force and mass

ISSN-L 2664-9969; E-ISSN 2706-5448

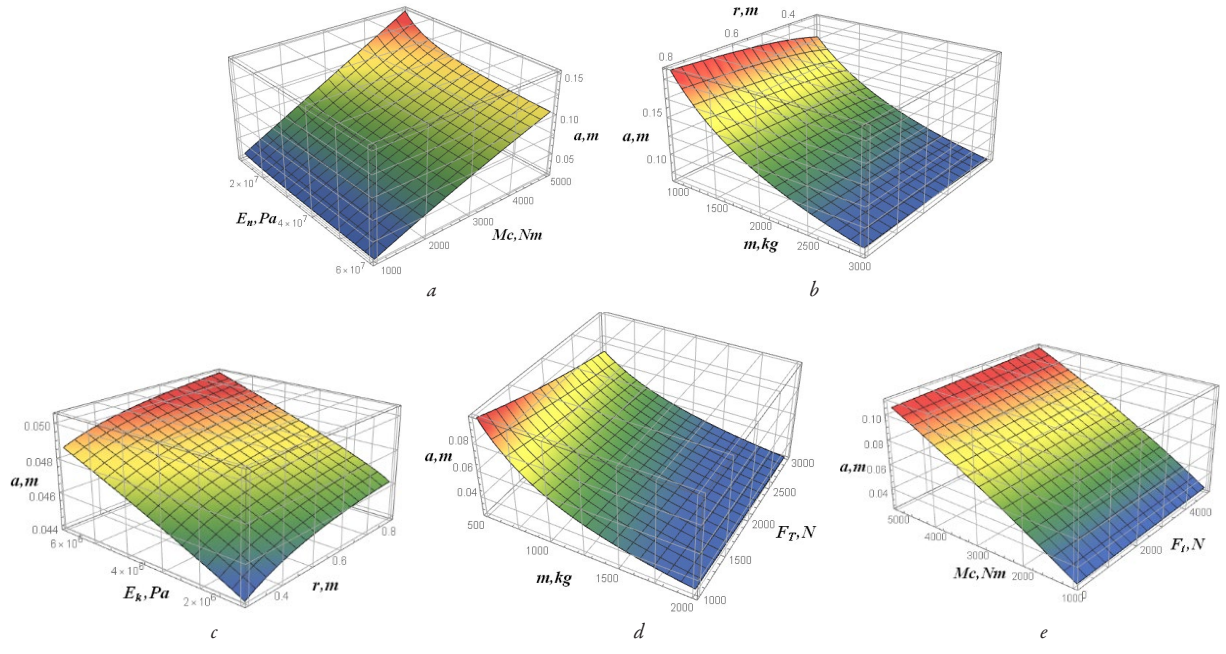

Fig. 7. Graphical representation of dependence of the front contact boundary coordinate *a* on key wheel parameters and properties: *a* – influence of wheel's curvature and applied torque; *b* – influence of wheel radius and mass; *c* – influence of wheel's modulus of curvature and radius; *d* – influence of traction force and mass; *e* – influence of applied torque and pushing force

The continued application of these research outcomes facilitates the optimization of tractive performance in mobile power units and allows for the prediction of permissible slip characteristics for wheeled machinery. Moreover, further utilization of the obtained results will contribute to reducing soil degradation caused by tractive power units, achieved by minimizing both horizontal and vertical shear deformations in the soil.

4. Conclusions

1. The absolute vertical deformation components for the tire and the support surface, which represent biharmonic analytical functions (F_{zkk}, F_{xkk}, h_k, F_{xnn}, F_{znn}, h), are the solution to the first boundary value problem for the plane formulation. Since the initial force distributions are functions of system loads, geometry, and material properties, the resulting deformation fields also depend on these same parameters.

2. The absolute vertical deformation of the wheel surface increases with an increase in applied torque M_c, tractive force F_T, and the system mass m distributed to the wheel. The absolute deformation of the support surface increases with an increase in any of the applied loads – including wheel torque M_c, tractive force F_T, pushing force F_t (for a passive wheel), and the mass m acting on the wheel. As expected, surface material with a higher modulus of elasticity is more resistant to indentation under load.

3. Horizontal deformations of the wheel surface increase with an increase in applied torque M_c, tractive force F_T, pushing force F_t (for a passive wheel), and the mass m acting on the wheel. This increase leads to horizontal deformation of the wheel, as it causes shear stresses in the contact zone. An increase in wheel torque M_c, tractive force F_T, pushing force F_t in the case of a passive wheel, and the mass m acting on the wheel also leads to more pronounced horizontal deformation of the support surface.

4. The final equations for determining the front and rear boundaries of contact are functions of the loads applied to the wheel, its geometric parameters, and the mechanical properties of both the wheel tire and the support surface. Research results obtained using continuum mechanics methods and solutions derived from mathematical physics methods enabled the determination of analytical relationships for the absolute deformation components of both the wheel surface and the support surface. These relationships allow for the determination of contact conditions to define the nature of the contact interaction between wheeled propulsion systems and the support surface. Compared to known solution methods based on theoretical mechanics, these methods account for the influence of deformations on the nature of the interaction, yielding more accurate and adequate results. Compared to experimental methods, the presented results are less labor-intensive and possess greater solution generality.

Conflicts of interest

The authors declare that they have no conflicts of interest in relation to the current research, including financial, personal, authorship, or any other, that could affect the research, as well as the results reported in this paper.

Financing

The research was conducted without financial support.

Data availability

All data are available, either in numerical or graphical form, in the main text of the manuscript.

Use of artificial intelligence

Grammarly (v.1.2.212.1789) – proofreading, editing. All proposed changes were checked by the authors and used based on their relative appropriateness.

Authors' contributions

Volodymyr Kovbasa: Conceptualization, Methodology, Writing – review and editing; ***Nataliia Priliepo***: Formal analysis, Visualization, Writing – original draft.

References

1. Johnson, K. L. (1985). *Contact Mechanics.* London: Cambridge University Press. https://doi.org/10.1017/cbo9781139171731
2. Kovbasa, V. P. (2006). *Mekhaniko-tekhnolohichne obgruntuvannia optymizatsii robochykh orhaniv z gruntom.* [Doctoral dissertation; Natsionalnyi universytet bioresursiv i pryrodokorystuvannia Ukrainy]. Available at: https://uacademic.info/ua/document/0506U000111#!
3. Guthrie, A. G., Botha, T. R., Els, P. S. (2017). 3D contact patch measurement inside rolling tyres. *Journal of Terramechanics, 69,* 13–21. https://doi.org/10.1016/j.jterra.2016.09.004
4. Yamashita, H., Jayakumar, P., Alsaleh, M., Sugiyama, H. (2017). Physics-Based Deformable Tire–Soil Interaction Model for Off-Road Mobility Simulation and Experimental Validation. *Journal of Computational and Nonlinear Dynamics, 13 (2).* https://doi.org/10.1115/1.4037994
5. Kushnarov, A. S., Kochev, V. I. (1989). *Mekhaniko-tekhnologicheskie osnovy obrabotki pochvy.* Kyiv: Urozhai, 144.
6. Johnson, W., Mellor, P. B. (1973). *Engineering plasticity.* London, New York: Van Nostrand Reinhold Co. Available at: https://www.scribd.com/document/489339320/Engineering-Plasticity-by-W-Johnson-and-P-B-Mellor-pdf
7. Kovbasa, V. P., Solomka, A. V., Spirin, A. V., Kucheruk, V. Yu., Karabekova, D. Zh., Khassenov, A. K. (2020). Theoretical determination of the distribution of forces and the size of the boundaries of the contact in the interaction of the deformable drive wheel with the soil. *Bulletin of the Karaganda University "Physics Series", 99 (3),* 62–72. https://doi.org/10.31489/2020ph3/62-72
8. Kovbasa, V., Priliepo, N. (2025). Determination of analytical dependencies of distributed forces in a deformable wheel – deformable surface contact zone. *Technology Audit and Production Reserves, 3 (1 (83)),* 6–12. https://doi.org/10.15587/2706-5448.2025.329471
9. Yang, W., Tiecheng, S., Yongjie, L., Chundi, S. (2016). Prediction for Tire – Pavement Contact Stress under Steady – State Conditions based on 3D Finite Element Method. *Journal of Engineering Science and Technology Review, 9 (4),* 17–25. https://doi.org/10.25103/jestr.094.04
10. Swamy, V. S., Pandit, R., Yerro, A., Sandu, C., Rizzo, D. M., Sebeck, K., Gorsich, D. (2023). Review of modeling and validation techniques for tire-deformable soil interactions. *Journal of Terramechanics, 109,* 73–92. https://doi.org/10.1016/j.jterra.2023.05.007

Volodymyr Kovbasa, *Doctor of Technical Sciences, Professor, Department of Mechanical and Electrical Engineering, Poltava State Agrarian University, Poltava, Ukraine, ORCID: https://orcid.org/0000-0003-4574-5826*

Nataliia Priliepo, *Department of Mechanical and Electrical Engineering, Poltava State Agrarian University, Poltava, Ukraine, e-mail: nataliia.pryliepo@pdau.edu.ua, ORCID: https://orcid.org/0000-0002-4182-7405*

✉*Corresponding author*